National Pharmaceutical Engineering Center for Solid Preparation in Chinese Herbal Medicine[1]; Key Laboratory of Modern Preparation of TCM[2], Ministry of Education; State Key Laboratory of Innovative Drug and Efficient Energy-Saving Pharmaceutical Equipment[3], Jiangxi University of Traditional Chinese Medicine, Nanchang, Jiangxi Province, People's Republic of China

Preparation and pharmacokinetics of bifunctional epirubicin-loaded micelles

Qiaobei Pan[1,#], Jing Zhang[2,#], Xiang Li[3,*], Xing Han[1], Qian Zou[3], Peng Zhang[2], Ying Luo[2], Yi Jin[1,*]

Received March 25, 2019, accepted June 7, 2019

**Corresponding authors: Xiang Li, State Key Laboratory of Innovative Drug and Efficient Energy-Saving Pharmaceutical Equipment, Jiangxi University of Traditional Chinese Medicine, Nanchang, Jiangxi Province, People's Republic of China*
Yi Jin, National Pharmaceutical Engineering Center for Solid Preparation in Chinese Herbal Medicine, Jiangxi University of Traditional Chinese Medicine, Nanchang, Jiangxi Province, People's Republic of China
[#]These authors contributed equally to the work

Pharmazie 74: 577-582 (2019) *doi: 10.1691/ph.2019.9059*

In this study, micelles were designed to deliver an antitumor agent and a fluorescent marker to a tumor site. The micelles simultaneously encapsulated epirubicin (EPI) and polyethylene glycol (PEG)-modified graphene quantum dots (GQDs-PEG), and employed a PEG-polylactic acid block copolymer amphiphilic block polymer as a nanocarrier. Fourier transform infrared spectroscopy and X-ray photoelectron spectroscopy were used to characterize the functional groups in the synthesized GQDs-PEG. A Malvern particle size meter and transmission electron microscopy were used to show that the particle size of the GQDs-PEG is approximately 2-9 nm, and that of the bifunctional EPI-loaded micelles (EPI-FIDCR) is 19.59±1.21 nm, with zeta potential at -22.87±0.85 mV. The EE% and DL% for EPI in EPI-FIDCR are 74.02±0.55 % and 3.78±0.28 %, respectively. The IC_{50} values of EPI-FIDCR and EPI solution (EPI-Free) for tumor cells were 7.03 μg/mL and 5.54 μg/mL, showing that EPI-FIDCR still maintained strong cytotoxicity. Fluorescence micrographs of HeLa cells incubated with GQDs-PEG and EPI-FIDCR for 6 h, respectively, show that only EPI-FIDCR could enter the cells. *In vitro* cellular uptake assays and an inhibition study indicated that EPI-FIDCR could deliver both EPI and GQDs-PEG into tumor cells, while maintaining an inhibitory effect similar to that of unencapsulated EPI. A pharmacokinetic study showed that EPI-FIDCR could persist in the circulation for a significant period of time. The $AUC_{0\rightarrow t}$ calculated for the EPI-FIDCR formulation was 159.5-fold compared with that of EPI-Free, based on its improved stability and prolonged blood circulation time. The EPI-FIDCR enables both fluorescence imaging and controlled drug-release, exhibits prolonged systematic circulation time and has potential for the treatment of cancer.

1. Introduction

One of the main obstacles in cancer chemotherapy is the biodistribution of the chemotherapeutic compound, which can lead to severe off-target side-effects and toxicity (Gibson et al. 2018; Wilson et al. 2017; Zhao et al. 2017; Zhang et al. 2014). Chemotherapy is an important method in treating cancer (Khvorova and Watts 2017). Epirubicin (EPI) is an anthracycline antibiotic and antitumor epimer of doxorubicin that has been used to treat a wide range of cancers, such as breast, lung, ovarian, gastric and bladder cancers (Abnous et al. 2017; Chen et al. 2017; Yang et al. 2015). However, EPI has substantial lethal effects on healthy cells and tissues, leading to myelosuppression, cardiotoxicity and allergic reactions. In addition to these factors, the dose-dependent effects of drug accumulation is a major issue which limits the clinical application of such drugs (Mahmood et al. 2018; Chida et al. 2018). In the past decade, polymer micelles developed from amphiphilic block copolymers have been favored as drug delivery systems (Zhang et al. 2015; Xin et al. 2016; Zhou et al. 2019). Micelles have two extinguished advantages, compared to other drug delivery strategies. Firstly, micelles come with relatively small hydrodynamic size less than 50 nm, which is better for high drug accumulation at the target site. In addition to enhanced permeability and retention (EPR) effect, micelles are also characterized by their simple drug formulation and feasible manufacturing (Lu et al. 2018). Polymer micelles are also ideal delivery systems for poorly soluble drugs and are widely used for many applications such as drug release, diagnostic preparations, and gene carriers (Pei et al. 2017; Kang et al. 2014; Zheng et al. 2014; Hpone Myint et al. 2016).

Graphene quantum dots (GQDs) are a new type of material that has been developed from graphene. The most obvious difference between GQDs and graphene is that the energy level band gap of GQDs is approximately 7 eV, compared with the energy band gap of graphene which is zero. This difference means that GQDs have a stronger edge effect and a smaller size effect, and their fluorescence quantum yield is significantly higher than that of graphene (Narasimhan et al. 2017). GQDs are approximately 10 nm in size, and not only retain the properties of graphene, that is, a large π bond, but also contain many characteristic light energy clusters that are introduced during synthesis, such as hydroxyl, carboxyl, and amino clusters (Bradley et al. 2017). Because of the toxicity of semiconductor quantum dots, their application in biological imaging is limited. In contrast, GQDs have good biocompatibility and stability, low cytotoxicity, and photobleaching resistance, and so they can replace semiconductor quantum dots in bioimaging applications (Schroneder et al. 2016; Li et al. 2018; Li et al. 2016). Appropriate surface modification of graphite-dilute quantum dots can effectively improve their luminescence properties such as

quantum yield and maintain the original properties of GQDs. The surface modification of GQDs can be performed through surface functionalization and surface doping (Chhabra et al. 2018; Pan et al. 2019). In the current paper, the carboxyl group on the surface of GQDs is reacted with the hydroxyl group of polyethylene glycol (PEG) to form a long-circulating material.

Although there is a substantial amount of prior research concerning long-circulation modified micelles for cancer treatment (Ouahab et al. 2014; Ma et al. 2018; Salzano et al. 2014; Li et al. 2016), few studies have combined micelles with fluorescent GQDs. Here, an amphiphilic block polymer based on a PEG-polylactic acid block copolymer (mPEG-PDLLA) was used as a nanocarrier, and it was loaded with EPI and PEG-modified GQDs simultaneously (Ouahab et al. 2014). We investigated the in vitro drug release of EPI-loaded micelles under different pH conditions, and performed a pharmacokinetic study of this bifunctional EPI-loaded micelles (EPI-FIDCR). The purpose of the current study was to reduce the toxicity of anticancer drugs and achieve fluorescence imaging in living organisms.

2. Investigations, results and discussion

2.1. Characterization of GQDs, GQDs-PEG and mPEG-PDLLA

As shown in Fig. 1, the GQDs demonstrate obvious absorption peaks at 3444 cm^{-1}(-OH) and 1079 cm^{-1} (stretching vibration of C-O in carboxyl groups), indicating the presence of carboxyl groups on the surface of the synthesized GQDs. The absorption peak at 2938 cm^{-1} corresponds to the stretching vibration of C-H, that at 1634 cm^{-1} corresponds to the stretching vibration of C=C, and that at 1731 cm^{-1}, 1401 cm^{-1} and 1216 cm^{-1}, corresponds to the stretching vibration of (C=O), (C-O) and (C-O-C), respectively. The introduction of oxygen-containing functional groups improves the aqueous properties of GQDs (Ahmed et al. 2018).

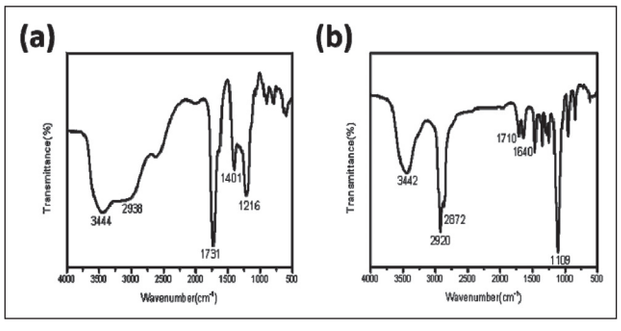

Fig. 1: FT-IR spectra of GQDs (a) and GQDs-PEG (b).

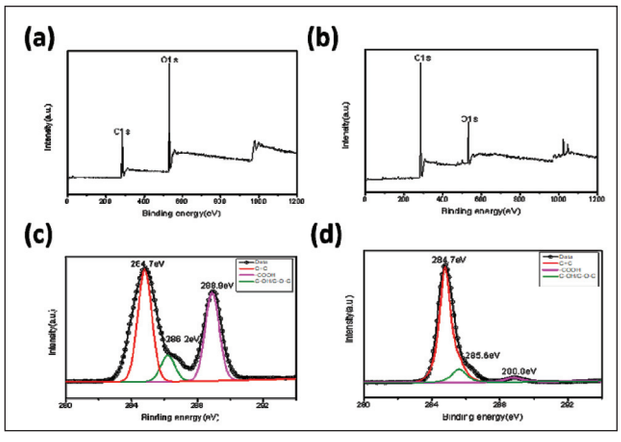

Fig. 2: Energy dispersive X-Ray spectroscopy of GQDs (a) and GQDs-PEG (b); C1s of GQDs (c) and GQDs-PEG (d)

Comparing the infrared spectra of GQDs and GQDs-PEG, it can be seen that the C-H characteristic absorption peaks of GQDs-PEG at 2920 cm^{-1} and 2872 cm^{-1} are important features of GQDs following mPEG bonding, and the peak intensity of the O-H characteristic absorption peak in GQDs-PEGs is reduced. The decrease in the intensity of the absorption peak and the peak intensity of the C=O bond at 1710 cm^{-1} are markedly weakened, and this indicates that mPEG bonds to the GQDs through dehydration synthesis.

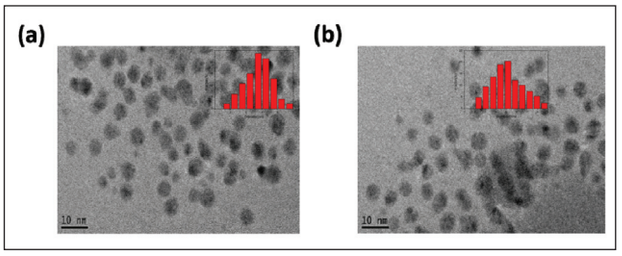

Fig. 3: TEM image of GQDs (a) and GQDs-PEG (b).

The composition of GQDs and GQDs-PEG was analyzed through XPS. Figure 2 (a) and (b) show full-scan XPS spectra of GQDs and GQDs-PEG, clearly showing the O1s signal and the C1s signal at 530 eV and 284 eV in a C1s high resolution XPS map of GQDs and GQDs-PEG. It can be seen from Figure 2 (c) and (d) that the GQDs have three distinct peaks at 284.7 eV, 286.2 eV, and 288.9 eV. The GQDs-PEG have three distinct peaks at 284.7 eV, 285.6 eV, and 288.8 eV, which correspond to C=C, C-OH/C-O-C and -COOH. The features of GQDs and GQDs-PEG are summarized in Fig. 3. During morphological characterization, spherical-shaped particles were observed. The GQDs and GQDs-PEG displayed a well-dispersed spherical morphology with a relatively uniform size. The TEM images showed that the GQDs were homogeneous and spherical in shape, with a size distribution range between 2–6 nm and a mean statistical diameter of 3.75 nm. The GQDs-PEG were homogeneous and spherical in shape, with a size distribution range between 2–9 nm and a mean statistical diameter of 4.81 nm. The increase in particle size could be explained by the materials intended to increase circulation time that surrounded the GQDs, which led to their larger size.

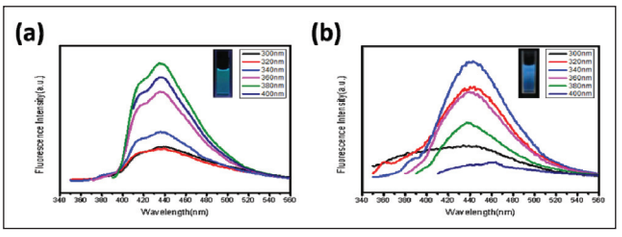

Fig. 4: Fluorescence spectra of GQDs (a) and GQDs-PEG (b) at different excitation wavelengths in the 300-400 nm range.

Figure 4 (a) and (b) show the fluorescence spectra of the GQDs and GQDs-PEG, respectively. The fluorescence images of the GQDs and GQDs-PEG under a 365 nm UV lamp show the samples as blue in color. The behavior of the GQDs at an excitation wavelength of 300–400 nm shows no dependence on the excitation wave length; that is, the emission wavelength does not change with a change in the excitation wavelength. The test found that the optimal excitation wavelength is 379 nm and the maximum emission wavelength is 435 nm. As can be seen from Fig. 4 (b), the GQDs-PEG have an optimum excitation wavelength of 338 nm and a maximum emission wavelength of 441 nm. Compared with the emission spectrum of the GQDs, the emission spectrum of the GQDs-PEG shows different degrees of red shift (that is, the direction of the wavelength shift), which indicates the growth of its grains.

2.2. *Characterization of the EPI-FIDCR*

The shape of the EPI-FIDCR were assessed through TEM, as presented in Fig. 5. The TEM images showed that the EPI-FIDCR were homogeneous and spherical in shape. The size and zeta potential for EPI-FIDCR were 19.59±1.21 nm and -22.87±0.85 mV, respectively. The EE% and DL% for EPI in EPI-FIDCR were 74.02±0.55 % and 3.78±0.28 %, respectively.

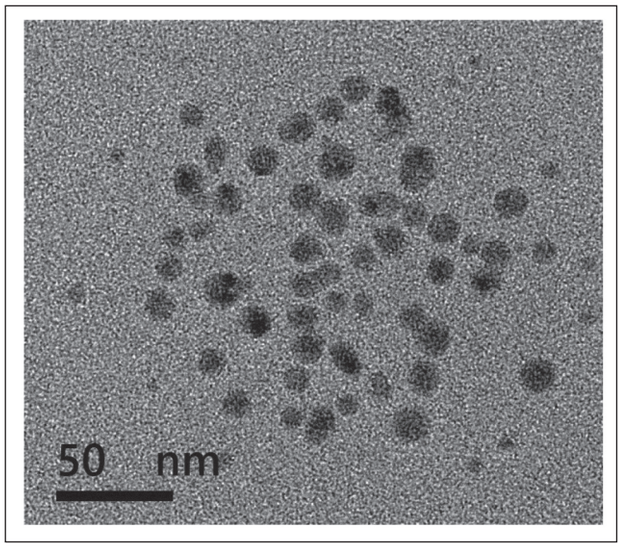

Fig. 5: Transmission electron micrographs (TEM) of EPI-FIDCR.

The AFM 3D image and topography image in Fig. 6 (a) and (b) indicate that the EPI-FIDCR particles are a spherical shape, which is consistent with the TEM results. As shown in Fig. 6 (c), the average height of the EPI-FIDCR is 22 nm, which is very close to the diameter observed using TEM and the zeta sizer. Therefore, we concluded that the EPI-FIDCR particles are monodisperse nanospheres with a size of approximately 20 nm.

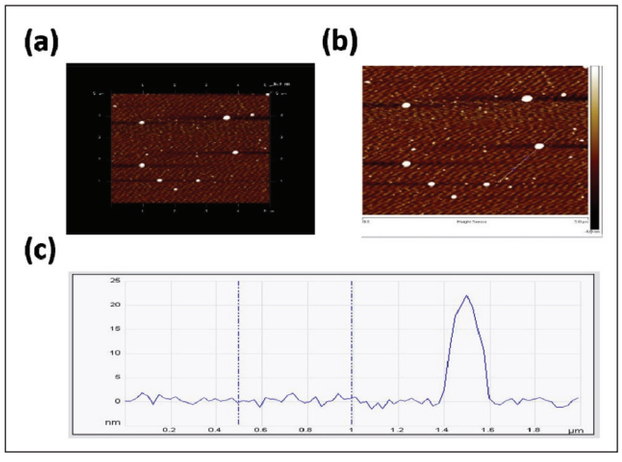

Fig. 6: AFM images of EPI-FIDCR. (a) AFM 3D image; (b) AFM topography image; (c) height profile along the line in (b).

The stability of micelles could be fundamentally improved by enhancing intra-micellar interactions, which are always reflected by the decreased CMC.13 As shown in Fig. 7, the CMC value of the EPI-FIDCR was determined as 3.8 mg/L (logC = −2.42) indicating that they display good stability upon strong dilution in blood circulation (Gaucher et al. 2010).

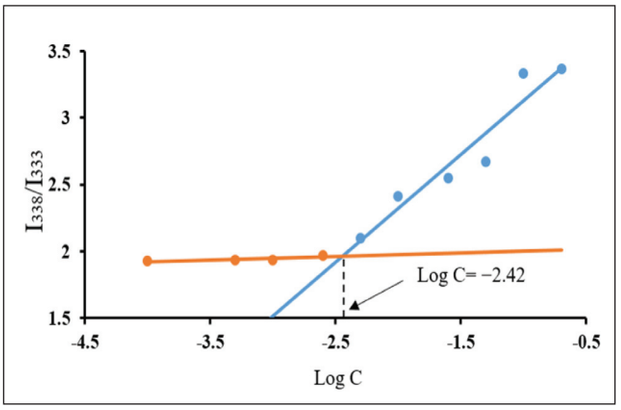

Fig. 7: CMC measurement of EPI-FIDCR.

2.3. *In vitro drug release assays*

The cumulative release of EPI from EPI-FIDCR and EPI-Free in different dissolution media over time is shown in Fig. 8 (a). The EPI-FIDCR showed a sustained release of EPI which is related to the pH value. During preparation, EPI hydrochloride was changed to its base form, and as a result, the encapsulation efficiency increased because of the increased hydrophobicity of the EPI. Therefore, the acid sensitivity of EPI-FIDCR in their release behavior comes from the addition of $NH_3 \cdot H_2O$ during the preparation process. With a decrease in pH value, the EPI release cumulative rate of EPI-FIDCR increased significantly. Under physiological pH (pH = 7.4), the free EPI was completely released by 12 h, and the cumulative release of EPI from EPI-FIDCR at 48 h was only 52.65 %. When the pH value changed to 6.5 and 5.0, which refer to a simulated tumor microenvironment or lysosome (Vaupel et al. 1989), the cumulative release of EPI of EPI-FIDCR increased to 64.81 % and 80.52 %, respectively. Furthermore, the f2 values for the formulations were calculated using the mean values of the cumulative release of EPI at every time point (Zhang et al. 2016). Values for f2 (50–100) indicates the equivalence between the two tested dissolution curves. The EPI-FIDCR had similar release profiles at pH 6.5 and 5.0 (Fig. 8 (b)), which indicates that the EPI-FIDCR was able to release incorporated EPI

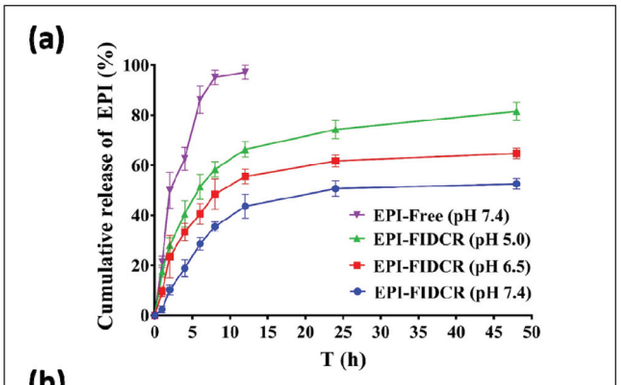

(b)

Comparisons	f2
EPI-Free/EPI-FIDCR (pH 7.4)	20
EPI-Free/EPI-FIDCR (pH 6.5)	26
EPI-Free/EPI-FIDCR (pH 5.0)	32
EPI-FIDCR (pH 7.4)/EPI-FIDCR (pH 6.5)	47
EPI-FIDCR (pH 6.5)/EPI-FIDCR (pH 5.0)	52

Fig. 8: (a) *In vitro* release curve of EPI-Free and EPI-FIDCR (n = 3); (b) f2 values for each comparison in PBS.

in tumor site environment and be disintegrated in the lysosome and released into the cell to exert the anti-tumor effect.

2.4. Cell viability studies

Cytotoxicity of the PEG-PDLLA, the GQDs-PEG nanoparticles, EPI-Free and the EPI-FIDCR in HeLa cells were investigated using an MTT assay (Table 1). The results showed that the PEG-PDLLA and GQDs-PEG nanoparticles exhibited no effect on cell viability, indicating their non-toxicity. Both EPI-Free and EPI-FIDCR showed almost the same toxicity to HeLa cells at 24 h, which was accordant to their IC_{50} in HeLa cells. The unaffected cell cytotoxicity of EPI in EPI-FIDCR and EPI-Free indicated that the preparation process of EPI-FIDCR did not impair the killing ability of EPI, which guarantee to play an anti-tumor effect *in vivo*.

Table 1: The IC_{50} values of different preparations after 24 h incubation (n=5)

Preparation	IC_{50} (μg/mL)
PEG -PDLLA	—
GQDs-PEG	—
EPI-Free	5.54±0.06
EPI-FIDCR micelles	7.03±0.03

—: not available

2.5. In vitro cellular uptake assays

The uptake of EPI-Free and EPI-FIDCR in HeLa cells was assessed by EPI-Free and EPI-FIDCR treatment for 2 h and 6 h, respectively, with the concentration of EPI at 10 μg/mL. As shown in Fig. 9, the EPI-Free only emitted red fluorescence after 6 h incubation with HeLa cells. The EPI-FIDCR can emit both red (EPI) and blue (GQDs-PEG) fluorescence in HeLa cells. As the incubation time increased, the fluorescence intensity of the EPI and GQDs-PEG in the EPI-FIDCR was significantly enhanced, indicating that the EPI in the EPI-FIDCR and GQDs-PEG can undergo cell uptake, thereby treating and labeling tumor cells.

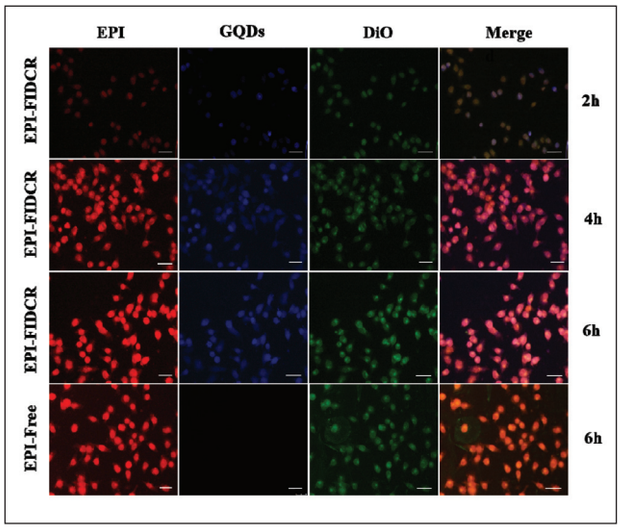

Fig. 9: Fluorescence micrographs of HeLa cells incubated with EPI-FIDCR and EPI-Free (From the left are EPI (red light), GQDs-PEG (blue light), DiO (cell membrane) and merge images (bar = 50 μm).

The red fluorescence intensity of the EPI-FIDCR and EPI-Free after incubation for 6 h in HeLa cells were almost the same, indicating that the micelle preparation procedure did not impair the EPI uptake in tumor cells.

2.6. Pharmacokinetic study of EPI-FIDCR

To fully describe the pharmacokinetics of the micelles, the *in vivo* blood clearance of the formulated micelles and EPI-Free was monitored and analyzed. The blood concentration-time curves after intravenous administration of the EPI-FIDCR or EPI-Free in rats are shown in Fig. 10. PKslover software was used for various compartmental analyses of all curves, and the relevant pharmacokinetic parameters, including the C_{max}, $AUC_{0\to t}$, $MRT_{0\to t}$, V_z and CL were determined using the corresponding compartmental analysis and are listed in Table 2. The EPI-loaded micelles exhibited a significantly prolonged blood drug concentration. The $AUC_{0\to t}$ calculated for the EPI-FIDCR formulation was 159.5-fold that of the free EPI. Furthermore, the EPI-FIDCR showed substantially slowed blood clearance within

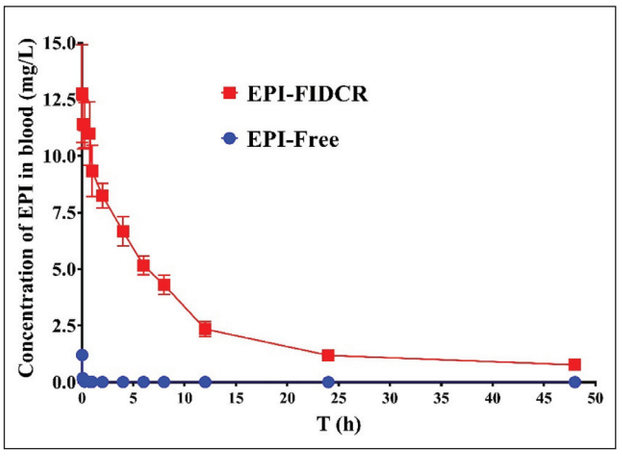

Fig. 10: Plasma concentration-time curve of EPI in EPI-FIDCR and EPI-Free after *i.v.* injection at 10 mg/kg (n=6).

Table 2: Pharmacokinetic parameters of EPI-FIDCR and EPI-Free after i.v. injection in rats (n=6)

Preparations	C_{max} (mg/L)	$AUC_{0\to t}$ (mg/L·h)	$MRT_{0\to t}$ (h)	Vz (L)	CL (L/h)
EPI-FIDCR	13.3±1.1	101.4±14.2	17.8±2.6	1.3±0.28	0.79±0.19
EPI-Free	1.2±0.2	0.6±0.1	423.5±38.3	830±96	1.9±0.4

the initial 12 h after intravenous administration, while the plasma clearance of the free EPI was 2.4 times that of the EPI-FIDCR. The physical properties of the EPI-FIDCR may contribute to this enhancement in their duration of circulation. PEG-modification of EPI-loaded micelles was found to be useful in shielding the nanoparticles from the RES because of steric repulsion (Gravel et al. 2013). PEG can form a hydrated outer shell, which can shield the nanoparticles from being recognized and eliminated by the RES. The effects of PEG result in an extended drug half-life and improved tissue distribution (Zhao et al. 2016). Although the obtained results might result from other more complicated mechanisms, the pharmacokinetic results showed that the EPI-FIDCR formulation had longer blood circulation compared with EPI-Free.

The current study reports the preparation and properties of EPI-FIDCR, which enable both fluorescence imaging and controlled drug-release, which is of great significance for the early diagnosis and visualization of a tumor. The EPI-FIDCR demonstrates a relatively uniform size and an acid-sensitive drug release behavior, maintaining a similar level of toxicity in HeLa cells with EPI-Free. The EPI-FIDCR not only demonstrates dramatically longer blood circulation than EPI-Free, but can also label tumor cells. The current study demonstrates promising multifunctional EPI-Free micelles for anti-tumor treatment.

3. Experimental

3.1. Materials

GQDs were purchased from Nanjing Xianfeng Nano Material Technology Co., Ltd (Jiangsu, China). Dichloro sulfoxide was purchased from China Pharmaceutical Group Chemical Reagent Co., Ltd (Shanghai, China). $mPEG_{2000}$ was purchased from Advanced Polymer Materials Inc (Canada, USA). EPI hydrochloride (>99 %) was purchased from Zhejiang Haizheng Pharmaceutical Co., Ltd (Zhejiang, China). An EPI standard reference (>99.9 %) was provided by Famasia Puqiang Co., Ltd (Shanghai, China). PEG_{2000}-PDLLA was purchased from Xian Ruixi Biological Technology Co., Ltd (Shangxi, China). Pyrene was purchased from Sigma-Aldrich (Sigma-Aldrich, MO, USA). Dialysis bags (MW cutoff: 3500 Da) were purchased from Shanghai Yuanye Biological Technology Co., Ltd (Shangxi, China). High-pressure liquid chromatography (HPLC)-purity grade methanol was purchased from Sigma-Aldrich Co. (St Louis, MO, USA). Daunorubicin hydrochloride (>99 %) was purchased from Famasia Puqiang Co., Ltd (Shanghai, China). DiO ($DiOC_{18}(3)$, 3,3'-Dioctadecyloxacarbocyanine perchlorate) was from Beyotime Biotechnology Co., Ltd (Shanghai, China). Distilled water was produced using a Milli-Q purification system (EMD Millipore, Billerica, MA, USA). All other chemicals were of analytical grade and were used as received.

3.2. Animals

Sprague-Dawley rats (female and male, 200±20 g) were provided by Hunan SJA Laboratory Animals (Hunan, China). All animal handling protocols were approved by the Institutional Animal Care and Use Committee of Jiangxi University of Traditional Chinese Medicine (Nanchang, China).

3.3. Cells

HeLa cell line was obtained from Beijing Dingguo Changsheng Biotechnology (Beijing, China). These cells were cultured in Dulbecco's modified Eagle's medium (DMEM, Life Technologies, Carlsbad, CA, USA) containing 10 % fetal bovine serum (Hyclone, Logan, UT, USA) and 1 % penicillin and streptomycin solution (Hyclone, Logan, UT, USA). Cells were cultivated under a humidified atmosphere at 37 °C and 5 % CO_2.

3.4. Synthesis and characterization of GQDs-PEG

GQDs (30 mg) were dissolved in 20 mL of dichloro sulfoxide and 0.5 mL of N, N-dimethylformamide (DMF) in a 50 mL eggplant-shaped flask and the reaction was stirred in an oil bath at 70 °C for 24 h. After the reaction was completed, the remaining $SOCl_2$ was removed, and a small amount of solvent was left to be drained using an oil pump. Subsequently, 0.12 g of $mPEG_{2000}$ and 20 mL of DMF were added, and the reaction was stirred for 2 d in an oil bath under nitrogen atmosphere. Finally, a 3500 Da dialysis bag was used to remove impurities, and the dialyzed solution was freeze-dried to obtain the GQDs-PEG in the form of a black powder.

Fourier transform infrared (FT-IR) spectra were obtained using a two FT-IR spectrometer (PerkinElmer, Waltham, MA, USA) with a resolution of 1 cm^{-1} in the range of 500–4000 cm^{-1}. Energy dispersive X-Ray spectroscopy was performed using a D8 ADVANCE (Bruker, Berlin, Germany) with an Al Kα X-ray source. A morphological examination of the GQDs and GQDs-PEG was performed using a JEM-1200 transmission electron microscope (TEM, JEOL, Tokyo, Japan) with an accelerating voltage of 200 kV. The GQDs and GQDs-PEG aqueous solutions were carefully dropped on a 200 mesh carbon film coated copper grid and dried at ambient temperature for TEM characterization. The size of the GQDs and GQDs-PEG was measured through dynamic light scattering, using a Zeta Sizer N (Malvern Instruments, Malvern, UK) at 25°C. The fluorescence spectra of the GQDs and GQDs-PEG were measured using an F-4500 fluorescence spectrophotometer (Hitachi, Tokyo, Japan).

3.5. Preparation and characterization of EPI-FIDCR

EPI hydrochloride (2 mg) was dissolved in 6 mL of acetonitrile, and 10 µL of triethylamine was added. The mixture was stirred for 10 min, and then 40 mg of PEG-PDLLA and 2 mg of GQDs-PEG were added to dissolve for 30 min with stirring, to form polymer micelles. The complexes were spin-evaporated in a water bath at 50 °C for 1 h to remove the organic solvent, and 2 mL of 0.9 % sodium chloride was added. The complexes were allowed to hydrate at 25 °C for 10 min, and then the suspension was filtered through a 0.22 µm organic filter to obtain EPI-FIDCR.

Encapsulation efficiency (EE%) and drug loading (DL%) were determined using an ultrafiltration technique to separate the non-encapsulated drug from the micelles. For this, a 500 µL EPI-FIDCR micelle dispersion was placed in an ultrafiltration tube (Nanosep MF; Pall Corporation, NY, USA), which was fitted with a filter membrane (MW cutoff: 10 kDa). The free drug in the underlying solution was collected through centrifugation at 3,340×g for 20 min (3–18 K high-speed refrigerated centrifuge; Sigma-Aldrich, Darmstadt, Germany), and the drug content in the ultrafiltrate (c_{free}) was determined through high performance liquid chromatography (HPLC) using a Welch Ultimate XB-C_{18} (250 × 4.6 mm, 5 µm; Yuexu Technology Co., Ltd, Shanghai, China) at 254 nm. The mobile phase was composed of 0.3% potassium dihydrogen phosphate–acetonitrile (3:7, v:v), and the flow rate was 1.0 mL/min. The column temperature was maintained at 25°C, and the injection volume was 10 µL. Then, 0.2 µL of the EPI-FIDCR micelle dispersion was diluted in 1.0 mL of methanol to determine the total drug concentration (c_{total}) through HPLC, and $M_{micelles}$ means the total mass of drug-loaded micelles. The EE% and DL% were calculated using Eqs. (1) and (2):

$$EE\% = (C_{total} - C_{free})/C_{total} \times 100, \quad (1)$$

$$DL\% = (C_{total} - C_{free})/M_{micelles} \times 100 \quad (2)$$

A morphological examination of the EPI-FIDCR was performed using a JEM-1200 EX electron microscope (JEOL, Tokyo, Japan) with an accelerating voltage of 200 kV. The EPI-FIDCR suspension was carefully dropped on a 200 mesh carbon film coated copper grid and dried at ambient temperature for TEM characterization. Atomic force microscopy (AFM) images were acquired using a Bruker Dimension Icon AFM in the tapping mode.

A fluorescent probe technique was employed to determine the critical micelle concentration (CMC) of the EPI-FIDCR using pyrene as a fluorescent probe (Hou et al. 2011). Briefly, 1 mL of 6×10^{-6} M pyrene solution in acetone was added to a series of 10 mL volumetric flasks and the acetone was subsequently evaporated using a nitrogen gas flow. The EPI-FIDCR solution was added to these volumetric flasks at different conjugate concentrations varying from 0.1 to 200 µg/mL. The combined solution of conjugate and pyrene was sonicated for 30 min, and then incubated at 65 °C for 1 h. After equilibration overnight at room temperature in the dark, the different samples were measured using a RF-5301 PC fluorescence spectrophotometer (Shimadzu, Japan). The intensity ratio I_{338}/I_{333} was plotted against the logarithm of conjugate concentration. The CMC value of the EPI-FIDCR was calculated from the intersection of the low concentration tangent and the high concentration tangent (Wang et al. 2014).

3.6. In vitro drug release study

The drug release profiles of the EPI-FIDCR and EPI solution (EPI-Free) were investigated using the dialysis method in PBS at pH 7.4, 6.5 or 5.5. In brief, the preparations (EPI concentration: 1 mg/mL) were dispersed in 5 mL of PBS and then were sealed in a dialysis bag (MW cutoff: 3500 Da). Subsequently, the dialysis bag was immersed in 200 mL of PBS at 37 °C with continuous shaking. At specific time intervals, 1 mL of the solution outside the dialysis bag was removed and replaced with the same volume of fresh PBS. All the samples were analyzed for the concentration of EPI by using HPLC as mentioned before (n=3). The value of f2 was obtained by a mathematical comparison and calculated according to the method previously reported (Koester et al. 2004).

3.7. In vitro analysis of cytotoxicity

The cytotoxicity of PEG-PDLLA, GQDs-PEG, EPI-Free and EPI-FIDCR against HeLa cells was assessed using the thiazolyl blue tetrazolium bromide (MTT) method. HeLa cells were seeded in 96-well plates at a density of 5×10^4 cells per well and incubated for 24 h. Then the culture medium was removed and fresh medium containing PEG-PDLLA, GQDs-PEG, EPI-Free or EPI-FIDCR at different concentration was added to each well. After 24 h of incubation, 10 µL of MTT solution (5 mg/mL) was added and further incubated for 4 h. Afterwards, the medium was discarded and 150 µL of dimethyl sulfoxide was added to dissolve the formazan precipitate, and the optical density of the solution was measured at 490 nm using a SpectraMax® M3 microplate reader (Molecular Devices, USA).

3.8. In vitro cellular uptake studies

The cellular uptake of EPI-Free and EPI-FIDCR was determined using a positive fluorescence microscope. HeLa cells were grown overnight at a density of 1×10^5 cells per well in 24-well plates. Subsequently, the cells were exposed to EPI-FIDCR for 2 h, 4 h and 6 h, and EPI-Free was incubated with the cells for 6 h. After the incubation, the cells were washed and fixed using 4 % paraformaldehyde (v/v) at room temperature for 15 min, followed by DiO staining for cell membrane for 10 min. Finally, the cells were washed three times, sealed onto a glass slide, and observed under Olympus IX81 inverted microscope. All measurements were performed in triplicate.

3.9. Pharmacokinetics of EPI-FIDCR

Six male rats and six female rats were divided into two groups, EPI-FIDCR and EPI-Free (administration dose: 10 mg/kg). Each group included three males and three females. The blood samples were collected from the rat retroocular venous plexus at 0.017 h, 0.083 h, 0.25 h, 0.75 h, 1 h, 4 h, 6 h, 8 h, 12 h, 24 h and 48 h. The plasma was isolated from the blood samples through centrifugation at 2,780 × g for 10 min in heparinized centrifuge tubes, and the supernatant was removed and stored at -80 °C before test.

Before test, 50 µL (1 µg/mL) internal standard (IS) working solution of daunorubicin hydrochloride in methanol was added to the 100 µL sample, followed by adding 650 µL methanol to precipitate the protein. The mixture was centrifuged at 8,350 g (HC-3018R High Speed Refrigerated Centrifuge; Anhui USTC Zonkia Scientific Instruments Co., Ltd, Anhui, China) for 10 min. The obtained supernatant was subjected to HPLC/mass spectrometry analysis for the detection of EPI by an LCMS-8040 Liquid Chromatograph triple quadrupole mass spectrometer equipped with an electronic spray ion source in the positive mode (Shimadzu Corporation, Kyoto, Japan).

The chromatographic separation was determined on a C_{18} Welch Ultimate column (50 × 2.1 mm, 1.8 µm). Gradient elution was used using solvent A (1% formic acid in water) and solvent B (acetonitrile) at 25 °C. The gradient program used was as follows: initial phase from 0 minute to 1.8 minute, a linear change from A-B (95:5, v:v) to A-B (40:60, v:v); from 1.8 min to 2.6 min, a linear change from A-B (40:60, v:v) to A-B (5:95, v:v); from 2.6 min to 2.8 min, a linear change to A-B (5:95, v:v); from 2.8 min to 4.0 min, linear change to A-B (95:5, v:v); from 4.0 min to 6.0 min, linear change to A-B (95:5, v:v).

The mass spectrometer was operated in multiple reaction monitoring mode. The MRM transitions of EPI and IS were m/z 544 → 130.1 and m/z 528.2 → 321.1, respectively. The ionization source conditions included a capillary voltage of 4 kV, a cone voltage of 50 V, and a desolvation temperature of 350 °C. Nitrogen was used as collision gas at a pressure of 50 psi.

The peak concentration (C_{max}), the in-vivo residence time ($MRT_{0\to t}$), the area under the plasma concentration-time curve from time zero to time t ($AUC_{0\to t}$), and clearance from the bloodstream (CL) and the apparent distribution volume (V_Z) were obtained by using PKsolver.

3.10. Statistical analysis

Statistical analysis was performed using a one-way analysis of variance with SPSS software. $P < 0.05$ was considered significant.

Acknowledgements: The authors thank the National Natural Science Fund of China (No. 81560575, 81760639, 81603054 and 81373347), the Project funded by Jiangxi Province Postdoctoral Science Foundation and Daily Fund (2016KY08, 2015RC30 and 2016RC34), the Natural Science Fund of Jiangxi Province (20171BAB215066, 20171ACB21074), the Jiangxi Province Outstanding Young Talents Program (20162BCB23034, 20171BCB23097), Young Jinggang Scholar of Jiangxi Province and "1050" program of Jiangxi University of TCM (Jing Zhang), Jiangxi BaiQianWan Talents Program (Xiang Li), the Project funded by China Postdoctoral Science Foundation (2016M602084), the Fund for First-Rate Discipline of Chinese materia medica (JXSYLXK-ZHYAO055, JXSYLXK-ZHYAO056, JXSYLXK-ZHYAO019), the Project funded by Jiangxi Provincial Health and Family Planning Commission (2016A008) and the Youth Foundation of Jiangxi Provincial Education Department (GJJ170748) for financial support.

Conflicts of interest: The authors declare no conflict of interest.

References

Abnous K, Danesh NM, Ramezani M, Lavaee P, Jalalian SH, Yazdian-Robati R, Emrani AS, Hassanabad KY, Taghdisi SM (2017) A novel aptamer-based DNA diamond nanostructure for in vivo targeted delivery of epirubicin to cancer cells. RSC Adv 7: 15181-15188.

Ahmed B, Kumar S, Ojha AK, Hirsch F, Riese S, Fischer I (2018) Facile synthesis and photophysics of graphene quantum dots. J Photoch Photobio A 364: 671-678.

Bradley SJ, Kroon R, Laufersky G, Röding M, Goreham RV, Gschneidtner T, Schroeder K, Moth-Poulsen K, Andersson M, Nann T (2017) Heterogeneity in the fluorescence of graphene and graphene oxide quantum dots. Microchimica Acta 184: 871-878.

Chen JF, Yu BX, Yu R, Ma L, Lv XY, Cheng Y, Ma Q (2017) Monoclonal antibody Zt/g4 targeting RON receptor tyrosine kinase enhances chemosensitivity of bladder cancer cells to epirubicin by promoting G1/S arrest and apoptosis. Oncol Rep 37: 721-728.

Chhabra VA, Kaur R, Kumar N, Deep A, Rajesh C, Kim KH (2018) Synthesis and spectroscopic studies of functionalized graphene quantum dots with diverse fluorescence characteristics. RSC Adv 8: 11446-11454.

Chida T, Miura Y, Cabral H, Nomoto T, Kataoka K, Nishiyama N (2018) Epirubicin-loaded polymeric micelles effectively treat axillary lymph nodes metastasis of breast cancer through selective accumulation and pH-triggered drug release. J Control Release 292: 130-140.

Gaucher G, Satturwar P, Jones MC, Furtos A, Leroux JC (2010) Polymeric micelles for oral drug delivery. Eur J Pharm Biopharm 76: 147-58.

Gibson TM, Li C, Armstrong GT, Srivastava DK, Leisenring WM, Mertens A, Brinkman TM, Diller L, Nathan PC, Hudson MM, Robison LL (2018) Perceptions of future health and cancer risk in adult survivors of childhood cancer: A report from the Childhood Cancer Survivor Study. Cancer 124: 3436-3444.

Gravel E, Thézé B, Jacques I, Anikumar P, Gombert K, Ducongé F, Doris E (2013) Cellular uptake and trafficking of polydiacetylene micelles. Nanoscale 5: 1955-1960.

Hou L, Fan Y, Yao J, Zhou JP, Li CC, Fang ZJ, Zhang Q (2011) Low molecular weight heparin-all-trans-retinoid acid conjugate as a drug carrier for combination cancer chemotherapy of paclitaxel and all-trans-retinoid acid. Carbohydrate Polym 86: 1157-1166.

Hpone Myint K, Brouwn JR, Shim AR, Wyslouzil BE, Hall LM (2016) Encapsulation of nanoparticles during polymer micelle formation: a dissipative particle dynamics study. J Phys Chem B 120: 11582-11594.

Kang Y, Ha W, Liu YQ, Ma Y, Fan MM, Ding LS, Zhang S, Li BJ (2014) pH-responsive polymer-drug conjugates as multifunctional micelles for cancer-drug delivery. Nanotechnology 25: 335101.

Khvorova A, Watts JK (2017) The chemical evolution of oligonucleotide therapies of clinical utility. Nat Biotechnol 35: 238-248.

Koester LS, Ortega GG, Mayorga P, Bassani VL (2004) Mathematical evaluation of in vitro release profiles of hydroxypropylmethylcellulose matrix tablets containing carbamazepine associated to beta-cyclodextrin. Eur J Pharm Biopharm 58: 177-179.

Li K, Zhao X, Wei G, Su Z (2018) Recent Advances in the cancer bioimaging with graphene quantum Dots. Curr Med Chem 25: 2876-2893.

Li Y, Wu ZY, Du D, Dong DL, Li YY (2016) A graphene quantum dot (GQD) nanosystem with redox-triggered cleavable PEG shell facilitating selective activation of the photosensitiser for photodynamic therapy. RSC Adv 6: 6516-6522.

Lu Y, Zhang E, Yang J, Cao Z (2018) Strategies to improve micelle stability for drug delivery. Nano Res 11: 4985-4998.

Ma H, Jiang C (2018) Dehydroascorbic acid and pGPMA dual modified pH-sensitive polymeric micelles for target treatment of liver cancer. J Pharm Sci 107: 595-503.

Mahmood SS, Patel RB, Butler J, Vaduganathan M (2018) Epirubicin and long-term heart failure risk in breast cancer survivors. Eur J Heart Fail 20: 1454-1456.

Narasimhan AK, Lakshmi SB, Santra TS, Ramachandra Rao MS, Krishnamurthi G (2017) Oxygenated graphene quantum dots (GQDs) synthesized using laser ablation for long-term real-time tracking and imaging. RSC Adv 7: 53822-53829.

Ouahab A, Shao C, Shen Y, Tu J (2014) Development and characterization of stabilized double loaded mPEG-PDLLA micelles for simultaneous delivery of paclitaxel and docetaxel. Drug Dev Ind Pharm 40: 860-868.

Pan QB, Zhang J, Xiang Li, Zou Q, Zhang P, Luo Y, Jin Y (2019) Construction of novel multifunctional luminescent nanoparticles based on DNA bridging and its inhibitory effect on tumor growth. RSC Adv 9:15042-15052.

Pei X, Luo F, Zhang J, Chen W, Jiang C, Liu J (2017) Dehydroascorbic acids-modified polymer micelles target cancer cells to enhance anti-tumor efficacy of paclitaxel. Sci Rep 7: 975.

Salzano G, Riehle R, Navarro G, Perche F, De Rosa G, Torchilin VP (2014) Polymeric micelles containing reversibly phospholipid-modified anti-survivin siRNA: a promising strategy to overcome drug resistance in cancer. Cancer Lett 343: 224-231.

Schroeder KL, Goreham RV, Nann T (2016) Graphene quantum dots for theranostics and bioimaging. Pharm Res 33: 2337-2357.

Vaupel P, Kallinowski F, Okunieff P (1989) Blood flow, oxygen and nutrient supply, and metabolic microenvironment of human tumors: a review. Cancer Res 49: 6449-6465.

Wang XY, Chen YH, Dahmani FZ, Yin LF, Zhou JP, Yao J (2014) Amphiphilic carboxymethyl chitosan-quercetin conjugate with P-gp inhibitory properties for oral delivery of paclitaxel. Biomaterials 35: 7654-7665.

Wilson MK, Pujade-Lauraine E, Aoki D, Mirza MR, Lorusso D, Oza AM, du Bois A, Vergote I, Reuss A, Bacon M, Friedlander M, Gallardo-Rincon D, Joly F, Chang SJ, Ferrero AM, Edmondson RJ, Wimberger P, Maenpaa J, Gaffney D, Zang R, Okamoto A, Stuart G, Ochiai K (2017) Fifth ovarian cancer consensus conference of the gynecologic cancer intergroup: recurrent disease. Ann Oncol 27: 727-732.

Xin JY, Tang JL, Bu M, Sun YH, Wang LH, Liu HZ (2016) A novel eye drop of alpha tocopherol to prevent ocular oxidant damage: improve the stability and ocular efficacy. Drug Dev Ind Pharm 42: 525-34.

Yang J, Zhang R, Radford DC, Kopeček J (2015) FRET-trackable biodegradable HPMA copolymer-epirubicin conjugates for ovarian carcinoma therapy. J Control Release 218: 36-44.

Zhao J, Xu Y, Wang C, Ding Y, Chen M, Wang Y, Peng J, Li L, Lv L (2017) Soluplus/TPGS mixed micelles for dioscin delivery in cancer therapy. Drug Dev Ind Pharm 43: 1197-1204.

Zhao C, Deng H, Xu J, Li S, Zhong L, Wu Y, Liang XJ (2016) "Sheddable" PEG-lipid to balance the contradiction of PEGylation between long circulation and poor uptake. Nanoscale 8: 10832-10842.

Zhang XR, Shi NQ, Zhao Y, Zhu HY, Guan J, Jin Y (2015) Deoxycholic acid-grafted PEGylated chitosan micelles for the delivery of mitomycin C. Drug Dev Ind Pharm 41: 916-26.

Zhang J, Chen Y, Li X, Liang X, Luo X (2016) The influence of different long-circulating materials on the pharmacokinetics of liposomal vincristine sulfate. Int J Nanomed 11: 4187-4197.

Zhang J, Li X, Huang L (2014). Non-viral nanocarriers for siRNA delivery in breast cancer. J Control Release 190: 440-450.

Zheng Z, Wang JL, Chen HL, Feng LB, Jing R, Lu MZ, Hu B, Ji JB (2014) Magnetic superhydrophobic polymer nanosphere cage as a framework for miceller catalysis in biphasic media. Chem Cat Chem 6: 1626-1634.

Zhou Y, Gao H, Zhu F, Ge M, Liang G (2019) Sensitive and rapid detection of aliphatic amines in water using self-stabilized micelles of fluorescent block copolymers. J Hazard Mater 368: 630-637.